A Bayesian Inference-Based Approach to Empirical Training of Strongly Coupled Constituent Models

G. S. Flynn
Los Alamos National Laboratory,
Los Alamos, NM 87545
e-mail: garrison@lanl.gov

E. Chodora
Mechanical Engineering,
Clemson University,
Clemson, SC 29634
e-mail: echodor@clemson.edu

S. Atamturktur
Architectural Engineering,
The Pennsylvania State University,
State College, PA 16801
e-mail: sez@psu.edu

D. A. Brown
Mathematical and Statistical Sciences,
Clemson University,
Clemson, SC 29634
e-mail: ab7@clemson.edu

Partitioned analysis enables numerical representation of complex systems through the coupling of smaller, simpler constituent models, each representing a different phenomenon, domain, scale, or functional component. Through this coupling, inputs and outputs of constituent models are exchanged in an iterative manner until a converged solution satisfies all constituents. In practical applications, numerical models may not be available for all constituents due to lack of understanding of the behavior of a constituent and the inability to conduct separate-effect experiments to investigate the behavior of the constituent in an isolated manner. In such cases, empirical representations of missing constituents have the opportunity to be inferred using integral-effect experiments, which capture the behavior of the system as a whole. Herein, we propose a Bayesian inference-based approach to estimate missing constituent models from available integral-effect experiments. Significance of this novel approach is demonstrated through the inference of a material plasticity constituent integrated with a finite element model to enable efficient multiscale elasto-plastic simulations. [DOI: 10.1115/1.4044804]

Keywords: statistical inference, empirical surrogate, Gaussian process model, model calibration, elasto-plastic deformation, multiscale, multiphysics

1 Introduction

The behavior of natural and engineered systems is governed by interactions of physical phenomena (i.e., thermal or mechanical), domains (i.e., fluid or structure), scales (i.e., micro or macro), or functional components (i.e., aircraft wings or hull). These complex systems may be decomposed into independent, isolated *constituent models*, each representing an individual phenomenon, domain, scale, or component [1]. With this approach, constituent models are first solved independently and then allowed to communicate with each other through iterative algorithms that exchange their inputs and outputs. For example, a numerical representation of a highly anisotropic granular material can be developed by coupling a macroscale finite element model to predict stress, which can then be used by a mesoscale plasticity model to predict plastic strain behavior [2,3]. The computational process of solving the response of a coupled system by means of iterative evaluations of separate constituents is known as partitioned analysis [4].[1]

Partitioned analysis is innately dependent upon the availability of domain knowledge to develop a computational model for each constituent. However, there are many engineering and science problems where it is not feasible to develop mechanistic models for all needed constituents due to lack of expert knowledge of the specific constituent physics as well as significant resources needed for code development. Such situations unavoidably result in an incomplete representation of the overall system. One solution is to augment the models with experimental data to account for missing constituents. Ideally, tests that isolate the missing constituent response (known as *separate-effect experiments*) are available and one can empirically develop an input–output relationship to emulate the missing constituent. If such separate-effect experiments are unavailable, however, making use of *integral-effect experiments* (that capture the full system, including all relationships between constituents) or *intermediate-effect experiments* (that capture select interdependencies, but not all) may be a feasible option [5]. However, a mathematical framework for empirically learning a missing constituent from integral-effect experiments is currently unavailable in the literature. Addressing this knowledge gap is the focus of this paper.

The ability to infer the functional form of a constituent from available integral-effect experiments will be a meaningful contribution for the field of multiscale, multiphysics modeling [6]. In particular, developing such a capability would have a high impact in advanced materials modeling where models are used to predict material performance in extreme conditions [7–11]. Multiscale material problems with clear separation of scales that contribute to the elastic and plastic components lend themselves particularly well to approaches using partitioned analysis [12]. Traditionally, in such applications, model developers determine dependent parameters based on small-scale, separate-effect experiments [13]. However, this approach is unreliable for complex materials where separate-effect experiments are not always feasible [14]. The goal of this paper is to generate *empirical approximations* of missing constituents (referred to henceforth as *empirical constituents*) to couple with existing numerical models (referred to henceforth as *computational constituents*) to enhance the modeling of strongly coupled problems.[2]

The method presented herein is based on inference of a functional representation of a missing constituent from integral-effect experiments, explicitly recognizing and incorporating uncertainties prevalent throughout the process. The remainder of this paper

[1]Conversely, monolithic analysis involves the development of a single code that requires all constituents to advance in time in a synchronous manner.

Manuscript received September 18, 2018; final manuscript received August 26, 2019; published online November 11, 2019. Assoc. Editor: Kevin Dowding.

[2]In this context, we define *weak coupling* as models with dependence in only one direction and *strong coupling* as models with two-way coupling where equilibrium equations are satisfied at the interface [15].

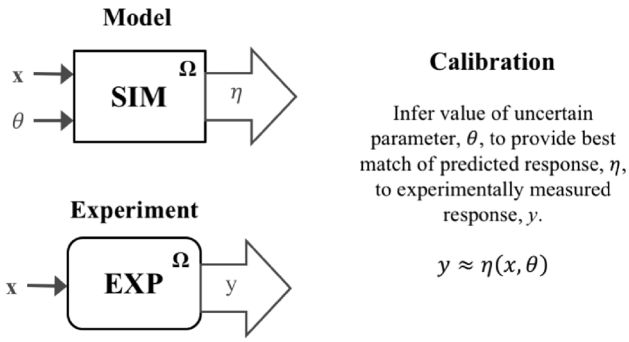

Fig. 1 Traditional calibration of stationary parameters

presents the details of the proposed functional inverse analysis and demonstrates its applicability through both academic and practical problems. Background discussion on the nature of strongly coupled models is presented in Sec. 2. Section 3 provides technical details on the Bayesian inference with consideration of the iterative nature of strongly coupled models. Section 4 details a case study of an elasto-plastic analysis in which the elastic behavior is captured by a finite element macroscale constituent, and the plasticity constituent is empirically inferred from integral-effect four-point bending test data. The inverse analysis and resulting plasticity constituent are presented in Sec. 5. Section 6 concludes with the significant findings, discussion of coupled systems for which the proposed methodology is ideally suited, and outlining a path forward for future work.

2 Perspectives on Model Calibration in Partitioned Analysis

Numerical models require input parameters to predict a system response. A subset of the model input parameters, however, may not have precisely known values. These parameters are referred to as uncertain parameters, θ. Uncertain parameters often relate to physical properties of a system, such as definitions of material characteristics and boundary conditions. The other important subset of model inputs is the control parameters, x, which designate the operational conditions of the system, such as temperature or applied load [16]. Model calibration is a method of inferring the values of uncertain parameters by comparing model predictions, η, to experimental measurements, y, of the same response at matched control parameter settings. Figure 1 illustrates traditional model calibration within a single domain, $\mathbf{\Omega}$. Using traditional calibration, a nominal value for θ is determined that achieves the best fit to all available data. Calibration parameters of this type will be referred to as *stationary parameters* for the remainder of the paper.

Consider a simple weakly coupled system, as shown in Fig. 2. The weakly coupled system has a one-way dependence in which the simulation for domain $\mathbf{\Omega}_2$ requires predicted data from the $\mathbf{\Omega}_1$ model as an input parameter. The prediction made by constituent domain $\mathbf{\Omega}_1$ is represented by η_1. Each domain also has a control input, x, and $\mathbf{\Omega}_2$ has an uncertain stationary parameter, θ. The response of the full system as predicted by the coupled model is η. Since this predicted response requires coupling of the constituents, it would be compared to an integral-effect experiment for calibration. The integral-effect experiments would be conducted in the coupled space, incorporating both $\mathbf{\Omega}_1$ and $\mathbf{\Omega}_2$. Now, let us pose the question: what if there is no constituent model available for $\mathbf{\Omega}_1$? With the constituent missing, the coupled model is incomplete and we are instead left with a only a simulation of $\mathbf{\Omega}_2$, referred to as the computational constituent. Here, we introduce a new type of uncertain parameter, known as a *functional parameter*, that serves to represent the functional form of the missing constituent model, $\varphi(x_\varphi)$. Contrary to the traditional stationary parameter, this new form of uncertain parameter will be calibrated so that its value is allowed to change as appropriate in relation to the relevant constituent domain control parameter. Such functional calibration has been demonstrated in Refs. [17] and [18].

Finally, consider the more complex extension of functional parameter calibration to a strongly coupled system, as shown in Fig. 3. The strongly coupled system has a two-way dependence where the simulation for domain $\mathbf{\Omega}_2$ requires predictions of the $\mathbf{\Omega}_1$ model as an input parameter and vice versa. Control inputs, x, and uncertain stationary parameters, θ, are now inputs to the coupled system rather than a specific model. In the same manner as the weakly coupled system, the goal is to achieve coupled model predictions, η, with the best match to measurements from integral-effect experiments, y. Again, consider the question: what if one of the constituent models is unavailable? We are then left with one computational constituent, $\mathbf{\Omega}_1$, with an uncertain input that is *dependent upon its own prediction*. The methodology proposed in this paper reframes this complex coupling uncertainty such that functional calibration can be extended for inference of a missing constituent model within a strongly coupled system. Once inferred, this empirical constituent model, represented as an

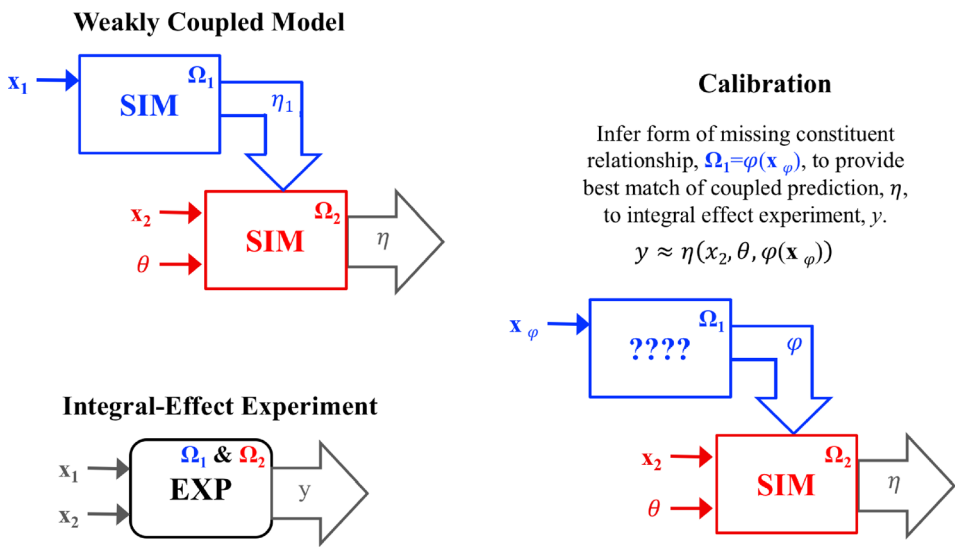

Fig. 2 Functional calibration for inference of a missing constituent model in a weakly coupled system

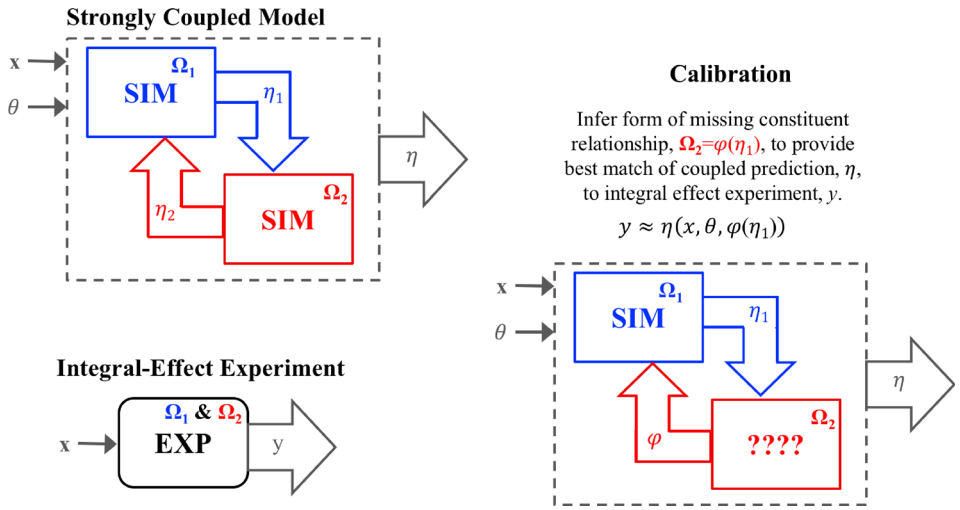

Fig. 3 Functional calibration for inference of a missing constituent model in a strongly coupled system

uncertain functional parameter, can be implemented in the computational constituent, resulting in a new, experimentally augmented partitioned model.

3 Methodology for Inferring Constituent Models in Strongly Coupled Systems

3.1 Conceptual Framework. The methodology presented in this paper seeks to empirically estimate the previously unknown representation of a missing constituent model in a strongly coupled framework. Figure 4 is a representation of the missing constituent shown in Fig. 3 with the assumption imposed that the response predicted by $\boldsymbol{\Omega}_1$ would be a control parameter for the missing domain, i.e., $\eta_1 = x_\varphi$. From this point forward, the parameter input to the coupling relationship (x_φ) will be designated as a special class of control parameter, the *functional control*. This assumption is necessary for the existing functional calibration methodology because predictions of the desired empirical constituent must have a control parameter on which it is functionally dependent. All other control parameters (x) do not change from the traditional approach and will be referred to as *system control* parameters. Implications of this assumption will be discussed further in Sec. 5.

Herein, the inference problem is posed such that the available physics-based constituent model is compared against associated integral-effect experiments. In this comparison, uncertain stationary parameters, θ, must also be taken into account to avoid the incorrect calibration of the functional parameter in compensation for incorrect values of the stationary parameter. Therefore, predictions of the coupled system, η, are represented as a function of x, θ, and $\boldsymbol{\varphi}(x_{\boldsymbol{\varphi}})$. Calibration of the stationary and functional

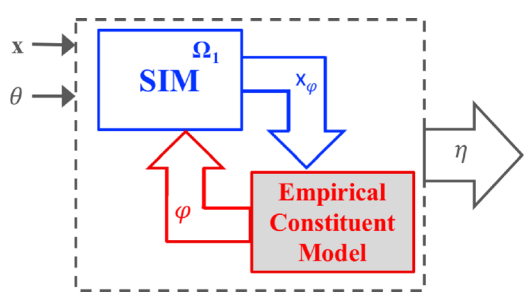

Fig. 4 Example system for demonstration of functional calibration

parameters takes place by optimizing the fit of model predictions to experimental measurements at N discrete control inputs while also taking into consideration experimental errors, ϵ, which are assumed to be independent and Gaussian distributed:

$$y(x^i) = \eta\left(x^i, \theta, \boldsymbol{\varphi}(x_{\boldsymbol{\varphi}})\right) + \epsilon_i \quad \text{for} \quad i = 1, 2, \ldots, N \tag{1}$$

where $\epsilon_i \sim N(0, \lambda_y^{-1})$. The measurement precision, λ_y, is typically treated as unknown and estimated from the data. Joint inference of uncertain parameters, θ and $\boldsymbol{\varphi}(x_{\boldsymbol{\varphi}})$, is necessary in this scenario to prevent unwarranted compensations between parameters. If a separate-effect experiment were to be available for the computational constituent, θ could be calibrated prior to $\boldsymbol{\varphi}(x_{\boldsymbol{\varphi}})$ inference. However, our focus in this paper is scenarios where the systems are so strongly coupled only integral-effect data is attainable therefore requiring joint inference.

3.2 Bayesian Modeling. We take a Bayesian approach to learning the form of the functional parameters, $\boldsymbol{\varphi}(x_{\boldsymbol{\varphi}})$, as well as the value for the stationary parameters, θ, so that both sources of uncertainties, as well as model and experimental uncertainties, may be considered simultaneously [17,18]. The Bayesian statistical paradigm proceeds by first representing any prior knowledge about unknown parameters and associated uncertainty through a *prior distribution*. The observed data are related to the unknown parameters through the assumed data-generating mechanism (i.e., the assumed probability distribution that the data came from, also called the *likelihood*). After obtaining the observed data, the prior distribution is updated with the information the data contains about the parameters to obtain the *posterior distribution*. Bayesian inference then proceeds by summarizing the posterior distribution; e.g., estimating the unknown parameters with the mean of the posterior distribution. For complex Bayesian models, the posterior distribution is typically simulated by sampling from it via Markov chain Monte Carlo (MCMC). A general exposition of Bayesian statistics may be found, for example, in Ref. [19].

In the case considered in this paper, if a functional form of the constituent model is known, a function with a known parametric structure can be imposed and the parameters estimated, such as that demonstrated in Ref. [20]. On the other hand, if even the parametric form of the function is unknown, one may prefer to use a *nonparametric prior* so that the functional form may be learned from the data. Gaussian process (GP) models are one example of such nonparametric models recommended as a well-suited, flexible alternative when the true form is not known [21,22]. Nonparametric models such as the GP make no

Table 1 Model parameter boundaries and prior distributions for Bayesian inference

		Minimum	Maximum	Prior distribution
	Ω_1 model parameters			
Control parameters	System control (x)	0	1	—
	Functional control (x_φ)	3	14	—
Uncertain model parameters	Stationary parameter (θ)	5	20	Uniform (5,20)
	Functional parameter [$\varphi(x_\varphi)$]	1	5	$\varphi(x_\varphi) \sim \mathrm{GP}\left(\boldsymbol{\mu}, \lambda_\varphi^{-1}\mathbf{R}\right)$
	GP empirical constituent hyperparameters			
Precision	λ_φ	—	—	Gamma (5,5)
Smoothness	ρ_φ	—	—	Beta (1,0.1)

assumptions about particular functional forms, thereby giving the data more freedom in determining the shape of the appropriate function. Similar to the way a Gaussian distribution is defined with a mean and standard deviation, a GP is defined with a mean and a covariance function. Any prior knowledge regarding the expected general tendencies of the functional form to be inferred (such as the degree of smoothness of the function) can be incorporated through the selection of the covariance function. The product power exponential covariance structure results in infinitely differentiable functions and hence is often preferred in applications thought to have smooth, continuous functional forms. This is often the case with the majority of mechanistic engineering systems and is, therefore, the covariance structure used in this work [22,23]. Other covariance structures may be implemented as is suitable for the application at hand. The GP covariance function will generally depend on so-called *hyperparameters*. In our case, these parameters determine the precision (i.e., how far a particular function tends to move away from the mean, denoted λ_φ) and the correlation length (i.e., how correlated or "smooth" points of the function near each are, denoted ρ_φ). See Ref. [22] for an overview of GPs.

In this paper, we avoid assuming a specific functional form for the unknown functional parameter (i.e., the empirical constituent) and assume a Gaussian process prior

$$\boldsymbol{\varphi}(\boldsymbol{x}_\varphi) \sim GP\left(\boldsymbol{\mu}(\boldsymbol{x}_\varphi), \lambda_\varphi^{-1}\mathbf{R}(\rho_\varphi, \boldsymbol{x}_\varphi)\right) \tag{2}$$

where $\boldsymbol{\mu}(\boldsymbol{x}_\varphi)$ is the mean function (i.e., a "default function" about which the GP varies), and $\mathbf{R}(\rho_\varphi, \boldsymbol{x}_\varphi)$ is the *correlation* function which, when multiplied by λ_φ^{-1}, yields the covariance function. The precision and correlation length parameters are themselves assigned hyper-prior distributions. It is usually sufficient to fix the mean function to be constant, and that is what we do here. The GP prior can also be augmented with any known constraints (e.g., monotonicity) that can be incorporated into posterior sampling. Such constraints can improve the ability to estimate unobserved constituents. Implementation of such constraints will be demonstrated with a mechanistic material model in Sec. 4. Employing a GP on $\boldsymbol{\varphi}(x_\varphi)$, predictions of the resulting semi-empirical partitioned model may be obtained from the posterior distribution and the assumed model in Eq. (1). To sample from the posterior distribution (and hence to estimate the unknown quantities), Gibbs sampling is implemented with Metropolis substeps for better convergence of $\boldsymbol{\varphi}(\boldsymbol{x}_\varphi)$ [17,24–27]. The reader is referred to Ref. [18] for discussion on the effects of subsampling the functional parameter.

3.3 Proof-of-Concept Demonstration. Consider the academic example in Fig. 4. Our aim is to infer the missing constituent model by calibrating simulation outputs, η, to a set of synthetic experimental data, y. The form of $\boldsymbol{\Omega}_1$ is known

$$\boldsymbol{\Omega}_1 = x_\varphi = 1.3\boldsymbol{\varphi}x^3 + 1.5\sin(\theta x) + 3 \tag{3}$$

where θ has a true value of 10. The true from of the missing constituent is

$$\boldsymbol{\varphi}(x_\varphi) = 10\sqrt{x_\varphi} - \frac{x_\varphi^2}{7} \tag{4}$$

Synthetic integral-effect experiments, y, are generated by Eq. (5) once values of Eqs. (3) and (4) are determined by Newton–Raphson iterations as well as the true value of θ.

$$y = \cos\left(\sqrt{\boldsymbol{\Omega}_1}\right) \tag{5}$$

To demonstrate the methodology, we assume the functional form of Eq. (4) and the value of the stationary parameter, θ, are not known. We seek to infer $\boldsymbol{\varphi}(x_\varphi)$ from a GP prior as well as the value of θ, where the prior on θ is taken to be uniform so that all values within a known range are assumed to be equally likely, a priori.

A GP with a constant mean of 0.5 and squared exponential covariance function dependent upon a precision hyperparameter, λ_φ and length hyperparameter, ρ_φ is used as a prior distribution on the functional form of $\boldsymbol{\varphi}(x_\varphi)$. Details on the boundaries and prior distributions for these parameters are provided in Table 1.

Posterior densities of the GP hyperparameters are shown in Fig. 5 and posterior draws for $\boldsymbol{\varphi}(x_\varphi)$ (generated using the GP with the hyperparameters from Fig. 5) and θ are shown in Fig. 6 with

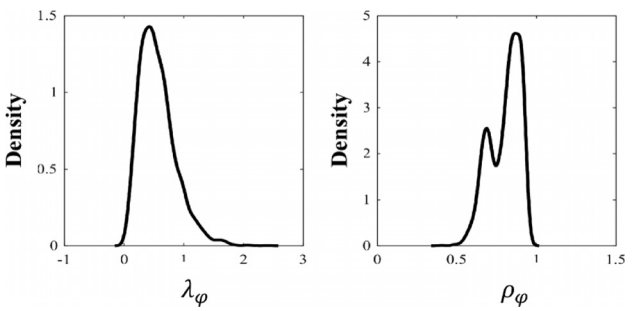

Fig. 5 GP hyperparameter posterior densities

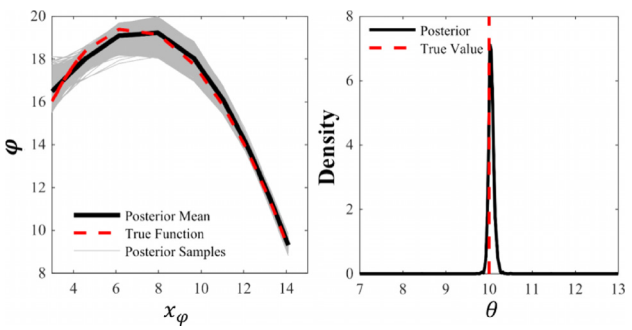

Fig. 6 Inferred functional parameter, $\varphi(x_\varphi)$, and constant parameter, θ, compared with true values used to generate synthetic integral-effect experiments

comparison of these inferred parameter values to the true parameter values. Once the GP representing the empirical constituent model for $\boldsymbol{\varphi}(x_{\boldsymbol{\varphi}})$ is determined, it is incorporated into the $\boldsymbol{\Omega}_1$ model to produce coupled predictions, which are shown in comparison to integral-effect experiments in Fig. 7. This example demonstrates the capability to infer both uncertain stationary parameter values as well as the important missing dependencies. Predictions made with the empirically inferred constituent illustrate the potential of our proposed approach to enable semi-empirical models of strongly coupled systems given only a single constituent and integral-effect data.

4 Multiscale Plasticity of Anisotropic Elasto-Plastic Material

4.1 Four-Point Bending of a Zirconium Beam. In this section, we apply the method discussed in Sec. 3 to infer the constituent material behavior of a zirconium beam [28]. The zirconium material exhibits a multiscale, elasto-plastic behavior. This behavior can be modeled by a macroscale finite element simulation for elasticity calculations coupled to a mesoscale calculating plastic strain components. In the following study we have a macroscale finite element model available but assume the mesoscale plasticity model is unavailable and must be inferred as an empirical model represented as a functional parameter. Figure 8 illustrates the coupling between the two scales as well as the classification of each parameter in the calibration context. The simulation control parameter is displacement applied to the beam over time, u. The macroscale anisotropic elasticity model predicts stress, σ, at every time step. If a mesoscale model were to be available it would take the macroscale stress prediction and in turn predict the plastic strain component, ε_{pl} [2,29]. Therefore, the goal of functional calibration is to obtain an empirical plasticity model as a stand-in for the mesoscale predictions, i.e., $\boldsymbol{\varphi}(x_{\boldsymbol{\varphi}}) \approx \varepsilon_{\text{pl}}(\sigma)$. When both scales are accounted for, the model predicts total strain, ε.

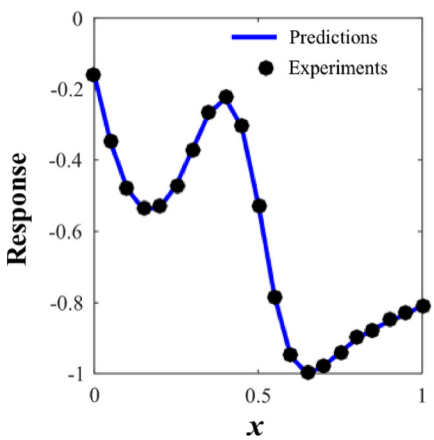

Fig. 7 Mean predictions of the calibrated semi-empirical model predictions $\eta(\boldsymbol{\Omega}_1, \boldsymbol{\varphi}, \theta, \boldsymbol{x})$

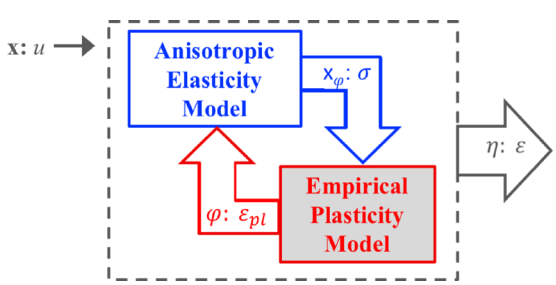

Fig. 8 Representation of multiscale coupling through empirically derived plasticity constituent model

The modeled beam has a 6.35×6.35 mm cross section and length of 50.8 mm. A four-point bending test is conducted in which supports under the beam are placed 12.7 mm from the centerline and vertical displacement of 10 mm is applied at two points 6.35 mm from the centerline (Fig. 9). An ABAQUS finite element model is used for the macroscale simulation with $32 \times 4 \times 4$ solid 20 node elements. The response of interest is total strain (combination of elastic and plastic) distribution in x and y components along the centerline of the beam face.

4.2 Integral-Effect Experiments. Synthetic experiments are generated using a fully coupled finite-element plasticity model (e.g., the macroscale model with the "true" form of the plastic constituent included in the coupling). The stress–plastic strain relationship used as the true function is shown in Fig. 10. In the remainder of this analysis, this constitutive relationship is assumed unknown and to be inferred from experimental data. Integral-effect data in the form of time-dependent strain measurements are synthetically generated using simulations of the previously described four-point bending test. Total strain is measured at nine locations on the face of the beam along the centerline. Measurements are taken continuously as the beam is loaded, resulting in a time series of total strain at every node. Integral-effect data at four moments in time are shown in Fig. 11.

4.3 Emulating Functionally Augmented Simulations. In a situation where the computer model is computationally demanding, it may be necessary to emulate the simulations to generate predictions rapidly. In our application, where the macroscale finite element model involves over 10,000 integration points, the computational demands of model evaluations in MCMC quickly become prohibitive. This limitation can be alleviated by a fast-running emulator. An emulator is trained using simulation runs available at a limited number of input settings and then implemented to estimate the simulation output at input settings where model evaluations are not available [30,31]. For this purpose, we use a GP in lieu of the physics-based finite element model with the mean predictions of this GP in place of the model predictions, η.

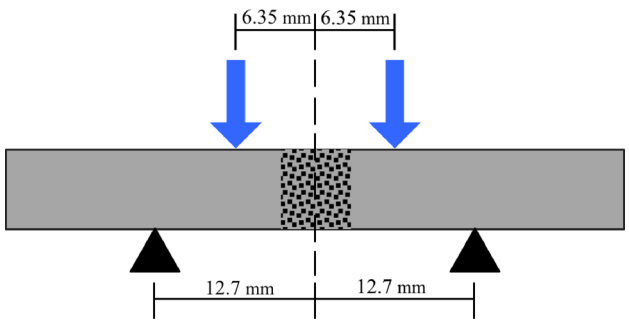

Fig. 9 Four-point bend test configuration

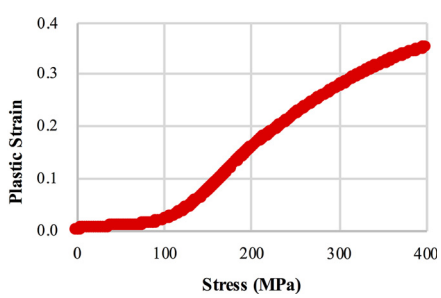

Fig. 10 Stress–plastic strain relationship used for the simulated experimental testing

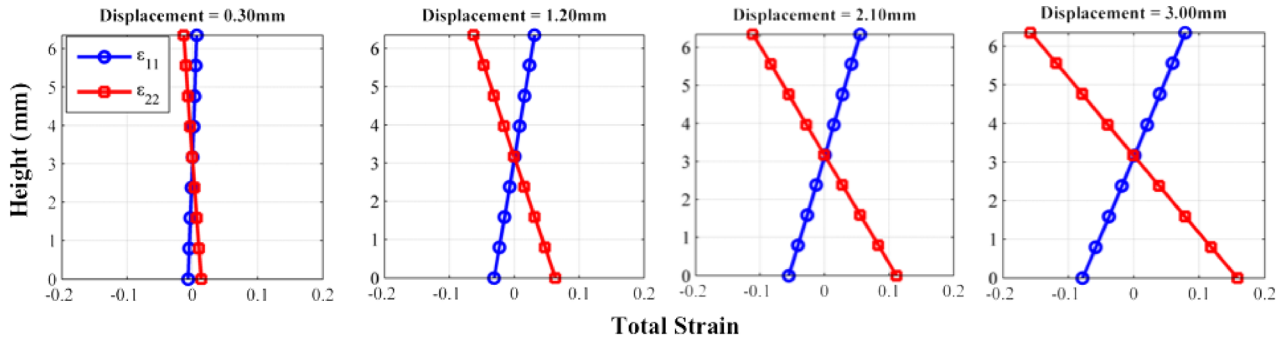

Fig. 11 Sample of integral-effect experiments capturing the midsection strain during loading

Table 2 GP hyperparameter ranges for generating emulator design of experiments

GP parameters	Minimum	Maximum
c	0.05	1.5
λ_φ	0.05	3.0
ρ_φ	0.80	1.0

4.3.1 Selection of Functional Parameter Design Points. While a large body of literature exists for generating efficient parameter design spaces for training emulators in which parameters are constant [32], the techniques for design of computer experiments to explore parameter spaces for training runs of functional parameters is limited. In applications such as our functional model calibration, the emulator must accept a function as input rather than a constant value to predict a model output that is representative of the simulations to be sampled during MCMC.

Consider, for instance, the case where the functional parameter $\boldsymbol{\varphi}(x_{\boldsymbol{\varphi}})$ is to be related to 50 settings of $x_{\boldsymbol{\varphi}}$. Values for these 50 points drawn randomly with no relation to each other would not accurately represent the functions to be sampled during calibration. Instead, the points should be related within the space achievable by the GPs defined smoothness and precision. Recently, Ezzat et al. [33] evaluate a series of sequential design techniques for functional emulator training. In our application, samples are drawn from the GP hyperparameters, $\lambda_{\boldsymbol{\varphi}}$ and $\rho_{\boldsymbol{\varphi}}$, and used to generate realizations of $\boldsymbol{\varphi}(x_{\boldsymbol{\varphi}})$. A parameter of random sample step size, c, is also included. The step size parameter defines the degree to which a realization is allowed to change from one sample to the next during the MCMC. Inclusion of step size in the emulator training ensures that all samples possibly generated during calibration will be bounded by the training domain. The resulting training set is a suite of functions feasibly obtained by the functional parameter's GP representation. GP hyperparameters allow for deviation from a baseline linear function, $\boldsymbol{\mu}_0$. Draws of $\boldsymbol{\varphi}(x_{\boldsymbol{\varphi}})$ follow the form shown in Eq. (6), where the covariance matrix is a squared exponential form parameterized by the smoothness parameter, ρ_φ (Eq. (7))

$$\boldsymbol{\varphi}(x_{\boldsymbol{\varphi}}) \sim \mathcal{N}\left(\mu_0, c\lambda_\varphi{}^{-1}\mathbf{R}\right) \tag{6}$$

$$\mathbf{R}(x_{\boldsymbol{\varphi}i}, x_{\boldsymbol{\varphi}j}) = \rho_\varphi^{4(x_{\boldsymbol{\varphi}i}-x_{\boldsymbol{\varphi}j})^2} \tag{7}$$

4.3.2 Emulator Training. A Latin hypercube design is used to select 400 runs given parameter ranges Table 2. The Gaussian processes for the machine learning (gpml) toolbox [22] is used to train the emulator by providing the functional inputs, $\boldsymbol{\varphi}(x_{\boldsymbol{\varphi}})$, and relevant cross-sectional strain outputs of the macroscale finite element model. Every third run is held out from the training set for the purpose of emulator cross validation. Cross validation is completed by comparing emulation predictions to model runs with the same input parameters. This cross validation is completed at all 20 of the displacement settings to assess the fidelity of emulator strain predictions. Cross validation results are shown in Fig. 12. Ideally, emulator strain predictions would match the finite element strain predictions given the same inputs simulation; in which case, all points in Fig. 12 would fall along the 45 deg line. As seen in the figure, the emulator and finite element model predictions fall closely along this line, providing confidence in the capability of the trained emulator to accurately represent the finite elemnt model with functional inputs. Since emulator predictions are generated by a GP they also include uncertainty, shown by error bars in Fig. 12.

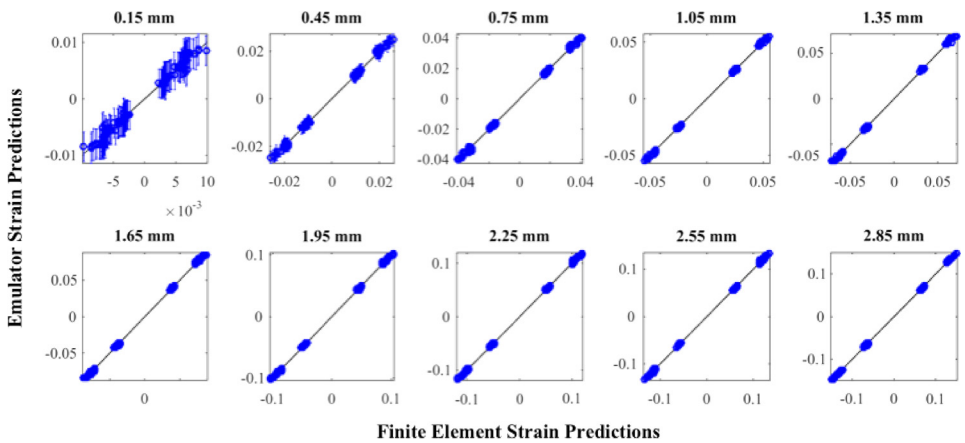

Fig. 12 Cross validation of GP emulator strain predictions by comparison with ABAQUS FE strain predictions at increasing displacements

Table 3 Parameter information and prior distributions for plasticity model inference

		Minimum	Maximum	Prior distribution
	Macroscale elastic model parameters			
Independent control, x	Displacement, u (mm)	0	10	—
Dependent control, x_φ	Stress, σ (MPa)	0	400	—
Functional parameter, φ	Plastic strain, ε_{pl}	0	0.5	$\varphi \sim \text{GP}\left(\boldsymbol{\mu}, \lambda_\varphi^{-1}\mathbf{R}\right)$
	GP empirical plasticity constituent hyperparameters			
Precision	λ_φ	—	—	Gamma (5,5)
Smoothness	ρ_φ	—	—	Beta (1,0.1)

Uncertainty is included at all of the displacements but becomes indistinguishable from the prediction at higher displacements because the uncertainty is orders of magnitude lower than predicted values.

4.4 Bayesian Inference on the Empirical Gaussian Process Plasticity Model. Finally, the methodology presented in Sec. 3 is applied to infer the functional form of the plasticity model, under the assumption that this constituent is unavailable. Table 3 details parameter ranges and prior distributions used in the functional Bayesian calibration.

Recall from Sec. 3.2 that a GP is desirable in Bayesian inference because it provides the flexibility of not imposing a functional form. GP models can also be made to satisfy appropriate constraints through transformation and/or truncation of the normal distribution. Furthermore, appropriate constraints may be placed as upper and lower bounds on the functional parameter value at any given $\boldsymbol{x}_{\boldsymbol{\varphi}}$ [17] or any other sampling point throughout the domain where information regarding the function is available. If general knowledge of the shape of the function is known, e.g., the function must be monotonic, then derivatives may be included in the covariance structure to better inform the sampled functional form [34]. In our study, the following known information is imposed on the GP model: (i) plastic strain is zero when the stress is zero; therefore, the function should be bounded to be negligible at low values; (ii) plastic strain should not exceed 0.5; therefore, the function should be bounded to a maximum of 0.5 across the entire domain; and (iii) plastic strain is irrecoverable by nature; therefore, the function should be monotonically increasing.

The first two constraints are implemented by bounding the samples so that no values outside these ranges at the appropriate areas of the domain can be drawn. The third constraint, monotonicity, is implemented by encouraging monotonic GP sampling as introduced in Ref. [34]. This constraint utilizes an expanded covariance matrix to learn about the derivatives of the GP. The new form of the covariance matrix is shown in Eq. (8), where $\mathbf{R}$ is the normal covariance function as defined by Eq. (7). Using this modified covariance, we take draws from a normal distribution with covariance including derivatives as well as a mean vector (Eq. (9)). In this mean vector, selected sampling locations, $\boldsymbol{x}'_{\boldsymbol{\varphi}}$, are not required to be the same as $\boldsymbol{x}_{\boldsymbol{\varphi}}$

$$\boldsymbol{\Sigma} = \begin{bmatrix} \mathbf{R}\left(x_{\varphi i}, x_{\varphi j}\right) & \dfrac{\partial \mathbf{R}}{\partial x_{\varphi_j}}\left(x_{\varphi i}, x_{\varphi j}'\right) \\ \dfrac{\partial \mathbf{R}}{\partial x_{\varphi_i}}\left(x_{\varphi i}', x_{\varphi j}\right) & \dfrac{\partial \mathbf{R}^2}{\partial x_{\varphi_i}\partial x_{\varphi_j}}\left(x_{\varphi i}', x_{\varphi j}'\right) \end{bmatrix} \tag{8}$$

$$\begin{bmatrix} \varphi^* \\ \varphi'^* \end{bmatrix} \sim \mathcal{N}\left(\begin{bmatrix} \varphi \\ \varphi' \end{bmatrix}, \lambda_\varphi^{-1}\boldsymbol{\Sigma}\right) \tag{9}$$

These draws result in a new sample of the functional parameter φ^*, as well as corresponding derivatives, φ'^*. A monotonicity indicator $m\left(\boldsymbol{x}'_{\boldsymbol{\varphi}}\right)$ is implemented that equals one when a derivative at a point $\boldsymbol{x}'_{\boldsymbol{\varphi}}$ is positive and zero if it is negative. Monotonic increase is then encouraged by applying $\boldsymbol{m}$ as a penalty term to the likelihood if the function is decreasing rather than increasing (Eq. (10)). For example, when φ'^* is negative at a given point, $\boldsymbol{m}$ will be equal to 0, making $\log(\boldsymbol{m})$ negative infinity, therefore causing the proposed value to always be rejected. However, when φ'^* is positive at a given point, $\boldsymbol{m}$ will be equal to 1, making $\log(\boldsymbol{m})$ equal to zero, thus having no effect on the log-likelihood. Further, the sampling is updated such that $\boldsymbol{\Sigma}$ is used in the place of $\mathbf{R}$ throughout the entire formulation and $\begin{bmatrix} \boldsymbol{\varphi} \\ \boldsymbol{\varphi}' \end{bmatrix}$ is used in place of $\boldsymbol{\varphi}$, except in the model evaluations

$$\log\left(\pi\left(\boldsymbol{\varphi}^*|\lambda_\varphi, \rho_\varphi, \boldsymbol{\varphi}\right)\right) = \frac{\lambda_y}{2}\left(y - \eta(\boldsymbol{\varphi}^*, \theta)\right)^{\mathrm{T}}\left(y - \eta(\boldsymbol{\varphi}^*, \theta)\right) - \frac{\lambda_\varphi}{2}\begin{bmatrix} \varphi^* - 0.5 \\ \varphi'^* \end{bmatrix}^{\mathrm{T}} \boldsymbol{\Sigma}^{\delta^{-1}} \begin{bmatrix} \varphi^* - 0.5 \\ \varphi'^* \end{bmatrix} + \log(\boldsymbol{m}) \tag{10}$$

Computation of the residual between measurements and predictions within the likelihood also accounts for the prediction precision, λ_y.

Constituent model inference is completed with 1000 burn-in runs and 1000 sampling runs, each with five subiterations of $\boldsymbol{\varphi}(\boldsymbol{x}_{\boldsymbol{\varphi}})$ [18,27]. Figure 13 shows all posterior draws of the functional parameter, as well as the mean and standard deviation of this distribution at control locations $\boldsymbol{x}_{\boldsymbol{\varphi}}$ compared to the true function (the plasticity model implemented to generate the integral-effect experimental data). The posterior distribution in these figures is shown within the plastic strain range of 0–0.5 to illustrate the reduction in uncertainty from the initial prior with a uniform distribution from 0 to 0.5. Posterior densities of the GP hyperparameters are shown in Fig. 14.

5 Results and Discussion

5.1 Multiscale Plasticity Calibration Results. The observed posterior distribution (Fig. 13) is populated primarily by linearly increasing functions, which aligns with the posterior density of $\rho_{\boldsymbol{\varphi}}$ strongly concentrated near 1, as well as the imposed monotonicity constraint. While it is typically desired to concentrate the density of $\rho_{\boldsymbol{\varphi}}$ to be close to 1 to impose smoothness in the function, the prior distribution heavily weighted to 1 in combination with the monotonicity constraint causing a trend in the functions to maintain positive derivatives, may be inducing restriction to functions approaching linearity in form. Even with this consideration, the trend of the true plastic strain form is captured within the credible interval throughout the domain. The pointwise mean of $\boldsymbol{\varphi}(\boldsymbol{x}_{\boldsymbol{\varphi}})$ follows a trend approximating the true function and matches most accurately in the region of highest plastic strain response, suggesting high plastic strain may be necessary for sufficient sensitivity to calibrate.

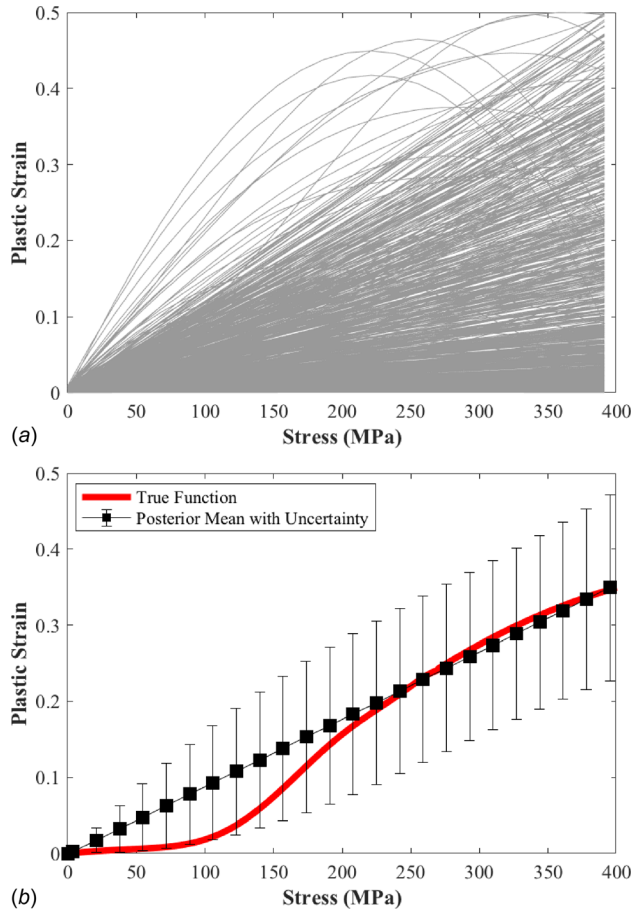

Fig. 13 Posterior draws (left) and summary (right) of the empirical plasticity constituent model compared to the true functional form

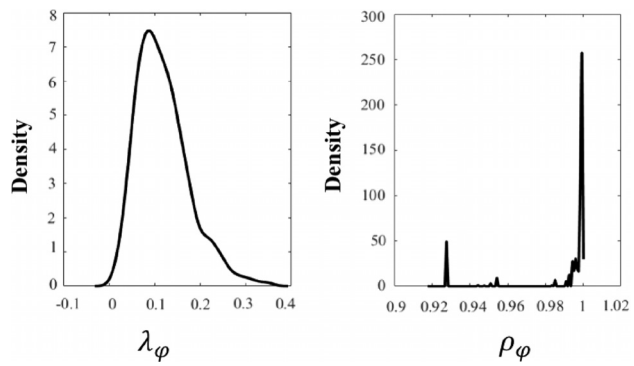

Fig. 14 Posterior densities of empirical GP model hyperparameters

Predictions of the finite element model augmented with the mean function of the inferred GP constituent model are shown in comparison to integral-effect experiments in Fig. 15, where points falling along the 45 deg line demonstrate the matching of calibrated predictions to integral-effect experimental data. Predictions are shown at four different heights of the beam midsection where integral-effect data were collected. The coupled predictions tend to match experiments reasonably well and are within 11% error, even at the outer fibers of the beam where the largest amount of plastic strain occurs during the testing. This is despite the fact that the mean function used to generate these coupled predictions is approximately linear, while the true plasticity function is nonlinear. This observation raises concern about sensitivity specific to the chosen model, especially in regions of low stress and low plastic strain, and leads to the slight overestimation of strain at the higher stress regions in Fig. 15. Overall, however, the coupled predictions serve as an appropriate representation of the experimental measurements and the underlying plasticity relationship.

5.2 Discussion of Methodology Applicability. We must consider the ways in which the nature of coupling a system with two-way dependence impacts applicability of the proposed methodology. In addition to control, x, and uncertain, θ, parameters let us introduce a new "general" input parameter, denoted as z [35]. For example, a material strength simulation may include a control input of load, x, an uncertain parameter of modulus of elasticity, θ, and a constant input parameter such as density, z, to predict displacement of a sample.

Considering these three classes of input parameters, Fig. 16 illustrates nine possible combinations by which dependent parameters can be shared between two strongly coupled constituent models. In this figure, the subscript letter denotes the model that is predicting a parameter to be input into the next model. Note that in all scenarios, uncertain parameters, θ, are not involved in the coupling. This is because, in our treatment, a dependent output of a constitutive model is not treated as an uncertain input parameter. It is a prediction of a constituent model, the system therefore has some knowledge of its value. This follows from the reasoning that any uncertainty in a dependent parameter will be mitigated by predicting the parameter value using the computational constituents.

The focus of the methodology proposed herein is on systems where the input to the constituent model that needs to be empirically inferred is a control input, x. As such, cases in which none of the dependent parameters fed into the missing constituent process are control parameters are not suited for inference through the mathematical framework presented. Expansion of the method for calibration opportunities where a control parameter is not involved in the iterative coupling is an exciting opportunity for future work.

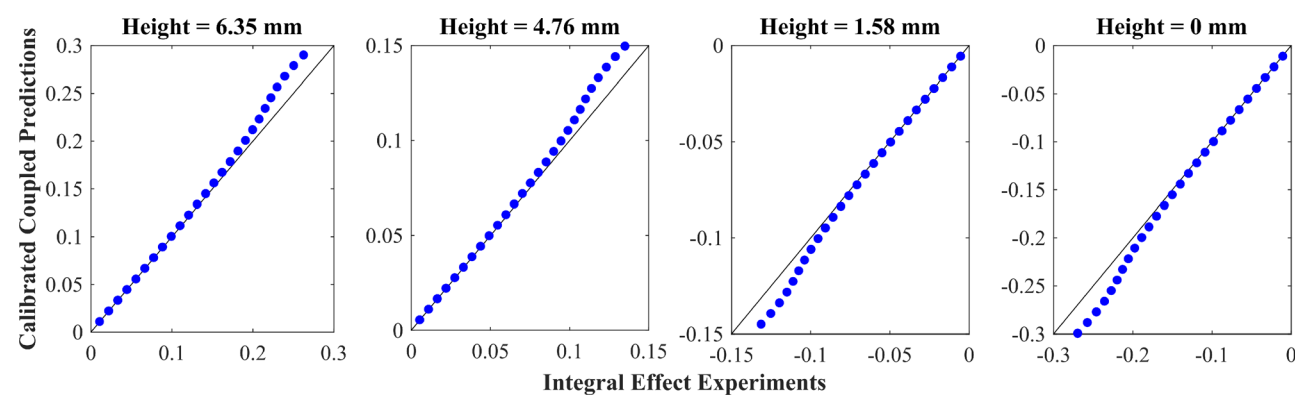

Fig. 15 Comparison of newly coupled model predictions and integral-effect experiments

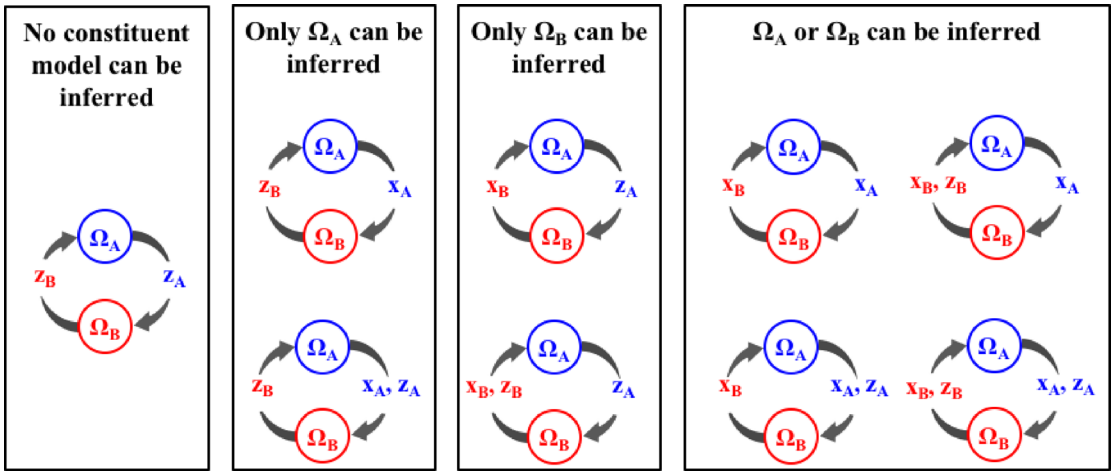

Fig. 16 Constituent model inference opportunities provided by the proposed methodology

6 Conclusions

Partitioned analysis provides model developers with the opportunity to represent the strongly coupled physical relationships observed in our complex engineering and science systems. Further, it provides the ability to leverage existing mature models of constituents within a system so that the focus of new model development efforts may be on the coupling among constituents rather than redeveloping already validated models with a monolithic approach. However, partitioned analysis is hindered when a constituent model is not available and conducting separate-effect experiments to empirically derive a constituent is not feasible.

This paper presents a statistical approach to infer the important coupling relationships between an existing physics-based model and its missing constituent through Bayesian inference utilizing integral-effect experimental data. The capability to infer the physics of a constituent model in the form of a functional input parameter, particularly for strongly coupled analysis, is unlike any other methodology existing today. The potential of the proposed methodology has been demonstrated with an academic example as well as development of a mesoscale plasticity model for representation of a multiscale elasto-plastic system.

While the results demonstrate the promise of this new method, there is clearly still work to be done. First, the physics-based constituents likely to be implemented in this inferential procedure will typically be too computationally demanding to evaluate thousands of times during the sampling steps, raising a need for emulators. Methods for generating sufficient design of experiments in functional parameter spaces, however, are not currently well-established. Producing a training dataset from a set of GP models with hyperparameters guiding the design selection has been demonstrated, but other approaches are still needed. Second, training of the constituent model form through GP model hyperparameters provides a combination of flexibility and control as the functional form is not restricted, but known constraints can be incorporated. The interaction of the prior information on the GP hyperparameters, such as encouraging monotonicity in the likelihood along with smoothness through the priors, is not yet well understood and should be further studied as methods continue to mature.

Funding Data

- U.S. Department of Education Graduate Assistance in Areas of National Need Program (Award No. P200A12022, Funder ID: 10.13039/100000138).

References

[1] Larson, J. W., 2009, "Ten Organising Principles for Coupling in Multiphysics and Multiscale Models," ANZIAM J., **48**, pp. 1090–1111.

[2] Knezevic, M., McCabe, R. J., Lebensohn, R. A., Tomé, C. N., and Mihaila, B., 2012, "Finite Element Implementation of a Self-Consistent Polycrystal Plasticity Model: Application to α-Uranium," Evolution, **100**, p. 2.

[3] Segurado, J., Lebensohn, R. A., LLorca, J., and Tomé, C. N., 2012, "Multiscale Modeling of Plasticity Based on Embedding the Viscoplastic Self-Consistent Formulation in Implicit Finite Elements," Int. J. Plast., **28**(1), pp. 124–140.

[4] Felippa, C. A., Park, K. C., and Farhat, C., 2001, "Partitioned Analysis of Coupled Mechanical Systems," Comput. Methods Appl. Mech. Eng., **190**(24–25), pp. 3247–3270.

[5] Unal, C., Williams, B., Hemez, F., Atamturktur, S. H., and McClure, P., 2011, "Improved Best Estimate Plus Uncertainty Methodology, Including Advanced Validation Concepts, to License Evolving Nuclear Reactors," Nucl. Eng. Des., **241**(5), pp. 1813–1833.

[6] Keyes, D. E., McInnes, L. C., Woodward, C., Gropp, W., Myra, E., Pernice, M., Bell, J., Brown, J., Clo, A., Connors, J., Constantinescu, E., Estep, D., Evans, K., Farhat, C., Hakim, A., Hammond, G., Hansen, G., Hill, J., Isaac, T., Jiao, X., Jordan, K., Kaushik, D., Kaxiras, E., Koniges, A., Lee, K., Lott, A., Lu, Q., Magerlein, J., Maxwell, R., McCourt, M., Mehl, M., Pawlowski, R., Randles, A. P., Reynolds, D., Rivière, B., Rüde, U., Scheibe, T., Shadid, J., Sheehan, B., Shephard, M., Siegel, A., Smith, B., Tang, X., Wilson, C., and Wohlmuth, B., 2013, "Multiphysics Simulations Challenges and Opportunities," Int. J. High Perform. Comput. Appl., **27**(1), pp. 4–83.

[7] Asayama, T., and Hasebe, S., 2000, "Weld Metal Creep–Fatigue Life Prediction by Modeling the Microstructure Degradation Due to the Exposure to High Temperature and Load," Nucl. Eng. Des., **195**(2), pp. 197–210.

[8] Dawson, P. R., 2000, "Computational Crystal Plasticity," Int. J. Solids Struct., **37**(1–2), pp. 115–130.

[9] McDowell, D. L., 2010, "A Perspective on Trends in Multiscale Plasticity," Int. J. Plast., **26**(9), pp. 1280–1309.

[10] Roters, F., Eisenlohr, P., Hantcherli, L., Tjahjanto, D. D., Bieler, T. R., and Raabe, D., 2010, "Overview of Constitutive Laws, Kinematics, Homogenization and Multiscale Methods in Crystal Plasticity Finite-Element Modeling: Theory, Experiments, Applications," Acta Mater., **58**(4), pp. 1152–1211.

[11] Panchal, J. H., Kalidindi, S. R., and McDowell, D. L., 2013, "Key Computational Modeling Issues in Integrated Computational Materials Engineering," Comput.-Aided Des., **45**(1), pp. 4–25.

[12] Wang, Y. B., Louie, M., Cao, Y., Liao, X. Z., Li, H. J., Ringer, S. P., and Zhu, Y. T., 2010, "High-Pressure Torsion Induced Microstructural Evolution in a Hexagonal Close-Packed Zr Alloy," Scr. Mater., **62**(4), pp. 214–217.

[13] Krätzig, W. B., and Pölling, R., 2004, "An Elasto-Plastic Damage Model for Reinforced Concrete With Minimum Number of Material Parameters," Comput. Struct., **82**(15–16), pp. 1201–1215.

[14] Bauer, T. H., and Holland, J. W., 1995, "In-Pile Measurement of the Thermal Conductivity of Irradiated Metallic Fuel," Nucl. Technol., **110**(3), pp. 407–421.

[15] Stevens, G., and Atamturktur, S., 2017, "Mitigating Error and Uncertainty in Partitioned Analysis: A Review of Verification, Calibration and Validation Methods for Coupled Simulations," Arch. Comput. Methods Eng., **24**(3), pp. 557–571.

[16] Hemez, F., Atamturktur, H. S., and Unal, C., 2010, "Defining Predictive Maturity for Validated Numerical Simulations," Comput. Struct., **88**(7–8), pp. 497–505.

[17] Brown, D. A., and Atamturktur, S., 2018, "Nonparametric Functional Calibration of Computer Models," Stat. Sin., **28**, pp. 721–742.

[18] Stevens, G. N., Atamturktur, S., Brown, D. A., Williams, B. J., and Unal, C., 2018, "Statistical Inference of Empirical Constituents in Partitioned Analysis From Integral-Effect Experiments: An Application in Thermo-Mechancial Coupling," Eng. Comput., **35**(2), pp. 672–691.

[19] Gelman, A., Carlin, J. B., Stern, H. S., and Rubin, D. B., 2014, *Bayesian Data Analysis*, Chapman & Hall, London.

[20] Atamturktur, S., Hegenderfer, J., Williams, B., Egeberg, M., Lebensohn, R. A., and Unal, C., 2015, "A Resource Allocation Framework for Experiment-Based Validation of Numerical Models," Mech. Adv. Mater. Struct., **22**(8), pp. 641–654.
[21] O'Hagan, A., 1978, "Curve Fitting and Optimal Design for Prediction," J. R. Stat. Soc., Ser. B, **40**(1), pp. 1–24.
[22] Rasmussen, C. E., and Williams, C. K. I., 2006, *Gaussian Processes for Machine Learning*, MIT Press, Cambridge, MA.
[23] Swiler, L. P., 2006, "Bayesian Methods in Engineering Design Problems," Sandia National Laboratories, Albuquerque, NM, Report No. SAND2005-3294.
[24] Metropolis, N., Rosenbluth, A. W., Rosenbluth, M. N., Teller, A. H., and Teller, E., 1953, "Equation of State Calculations by Fast Computing Machines," J. Chem. Phys., **21**(6), p. 1087.
[25] Hastings, W. K., 1970, "Monte Carlo Sampling Methods Using Markov Chains and Their Applications," Biometrika, **57**(1), p. 97.
[26] Geman, S., and Geman, D., 1984, "Stochastic Relaxation, Gibbs Distributions, and the Bayesian Restoration of Images," IEEE Trans. Pattern Anal. Mach. Intell., **PAMI-6**(6), pp. 721–741.
[27] Neal, R. M., 1998, "Regression and Classification Using Gaussian Process Priors," *Bayesian Stat*., J. M. Bernardo, J. O. Berger, A. P. Dawid, and A. F. M. Smith, eds., pp. 475–501.
[28] Kaschner, G. C., Bingert, J. F., Liu, C., Lovato, M. L., Maudlin, P. J., Stout, M. G., and Tomé, C. N., 2001, "Mechanical Response of Zirconium—II: Experimental and Finite Element Analysis of Bent Beams," Acta Mater., **49**(15), pp. 3097–3108.
[29] Stevens, G. N., Atamturktur, S., Lebensohn, R. A., and Kaschner, G. C., 2016, "Experiment-Based Validation and Uncertainty Quantification of Coupled Multi-Scale Plasticity Models," Multidiscip. Model. Mater. Struct., **12**(1), pp. 151–176.
[30] Kennedy, M. C., and O'Hagan, A., 2001, "Bayesian Calibration of Computer Models," J. R. Stat. Soc., Ser. B, **63**(3), pp. 425–464.
[31] Bayarri, M. J., Berger, J. O., Paulo, R., Sacks, J., Cafeo, J. A., Cavendish, J., Lin, C.-H., and Tu, J., 2007, "A Framework for Validation of Computer Models," Technometrics, **49**(2), pp. 138–154.
[32] Sacks, J., Welch, W. J., Mitchell, T. J., and Wynn, H. P., 1989, "Design and Analysis of Computer Experiments," Stat. Sci., **4**(4), pp. 409–423.
[33] Ezzat, A. A., Pourhabib, A., and Ding, Y., 2018, "Sequential Design for Functional Calibration of Computer Models," Technometrics, **60**(3), pp. 286–296.
[34] Golchi, S., Bingham, D. R., Chipman, H., and Campbell, D. A., 2015, "Monotone Emulation of Computer Experiments," SIAMASA J. Uncertain. Quantif., **3**(1), pp. 370–392.
[35] Farajpour, I., and Atamturktur, S., 2013, "Error and Uncertainty Analysis of Inexact and Imprecise Computer Models," J. Comput. Civ. Eng., **27**(4), pp. 407–418.